Fractured Reservoir Characterization using Azimuthal AVO

Burke J. Minsley, Daniel R. Burns, and Mark E. Willis
Earth Resources Laboratory
Dept. of Earth, Atmospheric, and Planetary Sciences
Massachusetts Institute of Technology
Cambridge, MA 02139

18 June 2003

Abstract

Ordinary least squares is used to investigate the ability to detect changes in physical properties using Amplitude Versus Offset (AVO) information collected from seismic data. In order to characterize vertically aligned fractures within a reservoir, this method is extended to Azimuthal AVO (AVOA) analysis. Azimuthal AVO has the potential not only to detect fractured zones, but to spatially describe the fracture strike orientation and changes in fracture or fluid properties. Depending on the data acquisition geometry, signal-to-noise ratio, and extent of fracturing, AVOA analysis can be marginally successful. A study of the robustness and limitations of AVOA analysis is therefore first classified with synthetic data. These methods are then applied to seismic data collected during an Ocean Bottom Cable (OBC) survey over a known fractured reservoir.

1 Introduction

1.1 Objectives

A common problem with geophysical data interpretation involves finding a robust method for clearly extracting subtle features from large, and possibly complicated, datasets. Amplitude versus offset analysis is a fairly well-used technique in the field of exploration seismology, as it has the ability to numerically describe features within the data that are not otherwise apparent. The methods for using AVO as an analysis tool are relatively straightforward, though results can be obscured by the many complications involved with analysis of field data. This case study will investigate the capabilities and limitations of azimuthal AVO as a tool for the detection and characterization of fractured reservoirs.

The fracture model is limited to vertical features that are aligned at a preferred orientation, which is commonly the situation in reservoir settings controlled by regional tectonic stresses. This fracture geometry is referred to as Horizontal Transverse Isotropy (HTI), as the fractures are transversely isotropic with a horizontal axis of symmetry. Extension to AVOA is very appropriate, as it allows for the simultaneous analysis of seismic data collected at different azimuths relative to the fractures. Inversion for AVO parameters related to the fracture orientation and elastic properties will be better constrained through this holistic approach, though a calibration of this method is necessary to understand the ability to resolve individual model parameters in the presence of imperfect data.

As a first order detection tool, AVOA analysis should be able to find the primary orientation of the fractures, as well as some quantification as to the degree of fracturing, which is measured essentially as an anisotropic AVO behavior. A secondary level of analysis should describe spatial differences in the physical properties of the fractures and saturating fluid such as fracture density, aperture, and elastic moduli. The ability to determine these properties is not straightforward, as they are coupled together within the AVO model parameters and can be easily biased.

The promise of using AVO as a reconnaissance/analysis tool with regards to fracture properties is quite attractive, as it is a relatively inexpensive addition to the typical acquisition and processing of seismic data.

Analysis of a 3D dataset also allows for a spatially continuous model of the fractures, which might otherwise only come from sparsely sampled well logs. Because AVO parameters can be related to fracture geometry and rock/fluid elastic properties, this analysis has the potential to infer some information about fluid saturation and flow.

1.2 Background

The underlying concept behind AVO was first generally developed by Knott and Zoeppritz near the beginning of the 20^{th} century. They described the reflection coefficient at an interface as a function of angle of incidence and the elastic properties of upper and lower materials. Simplifications of the general Zoeppritz equations have since been made that are applicable to the relatively subtle changes found in Earth materials at angles of incidence commonly used in exploration seismology. The linear approximations made by Aki and Richards (1980) and Shuey (1985) provide the basis for the AVO model used here. An extension of the Shuey method which describes AVOA for the HTI case was made by Rüger (1997).

There are many examples of techniques used for measuring response of fractured reservoirs using AVO, as well as some other velocity-analysis oriented methods. While much of the work is based on theoretical models, there is also a large amount of AVO analysis performed on field data, particularly in the exploration industry. Mallick et al. (1998) used a method similar to Rüger for describing the azimuthal variations of AVO over an area known to exhibit vertically aligned fractures. A more recent work by Dong and Davidson (2003) addresses the issue of 3D survey geometry and its implications for the adequacy of AVOA analysis.

1.3 Approach

To begin, a synthetic two-layer model is studied in order to understand the estimates and assumptions commonly made with simple least squares inversion methods applied to AVO analysis. The effects of these estimations, as well as geometry and noise considerations, will be taken into account. Building on this knowledge, the synthetic model will be extended to an HTI regime in order to use a similar analysis of the Rüger approximation. These techniques can then be applied to seismic datasets with a better understanding of their limitations. A particular example from an OBC dataset will be used to explore the reliability of this approach. A discussion of the synthetic results compared with the actual data analysis should help to capture the success of these methods, as well as focus the needs for future improvements.

2 Development

2.1 AVO approximation

It is useful to begin with a description of Shuey's form of Aki and Richard's approximation to the Zoeppritz equations.

$$R_{PP}(\Theta) \approx R_P + [A_0 R_P + \frac{\Delta\sigma}{(1-\sigma)^2}] \sin^2\Theta + \frac{1}{2}\frac{\Delta V_P}{V_P}(\tan^2\Theta - \sin^2\Theta) \tag{1}$$

where,

$$R_P = \frac{\rho_2 V_{P2} - \rho_1 V_{P1}}{\rho_2 V_{P2} + \rho_1 V_{P1}} \tag{2}$$

$$A_0 = B_0 - 2(1+B_0)\frac{1-2\sigma}{1-\sigma} \tag{3}$$

$$B_0 = \frac{\frac{\Delta V_P}{V_P}}{\frac{\Delta V_P}{V_P} + \frac{\Delta\rho}{\rho}} \tag{4}$$

and,

$R_{PP}(\Theta)$ is the angle of incidence-dependent reflectivity

Θ is the incidence angle of an incoming plane wave
$\sigma = \frac{(\sigma_2+\sigma_1)}{2}$ (σ is Poisson's ratio, and can be written in terms of V_P and V_S)
$\Delta\sigma = \sigma_2 - \sigma_1$
$\Delta V_P = V_{P2} - V_{P1}$
$V_P = \frac{(V_{P2}+V_{P1})}{2}$
$\Delta\rho = \rho_2 - \rho_1$
$\rho = \frac{(\rho_2+\rho_1)}{2}$

Equation 1 can be written as a linear equation in three parts, commonly given in terms of AVO coefficients A, B, and C.

$$R_{PP} \approx A + B\sin^2\Theta + C(\tan^2\Theta - \sin^2\Theta) \tag{5}$$

The A term, equal to R_P, describes the normal incidence ($\Theta = 0$) reflectivity, while the $\sin^2$ term applies to angles of incidence up to about 30 degrees, and the $(\tan^2 - \sin^2)$ term dominates for angles mostly above 30 degrees. This last term is sometimes disregarded in AVO analysis because these angles of incidence are larger than those used in most exploration surveys, though it still can play an important role.

Each term involves a combination of elastic parameters, a fact that will later define the ability to classify material changes through AVO model parameters. Also, note that R_{PP} is meant to represent the actual value of the reflection coefficient in equation 1. This is a difficult quantity to obtain with reflection seismic data; actual reflection amplitudes are often used instead as they are directly proportional to the reflection coefficient. This approximation further degrades the ability to use AVO as a quantification tool with regards to material properties, though careful calibration can be used to give some estimation of them.

2.2 Extension to AVOA in HTI media

Equation 5 describes the reflection amplitude dependence as a function of offset (or angle of incidence) and elastic parameters for an isotropic medium. For the HTI model,a set of vertically aligned fractures embedded in a homogeneous background material, shown in figure 1, is used.

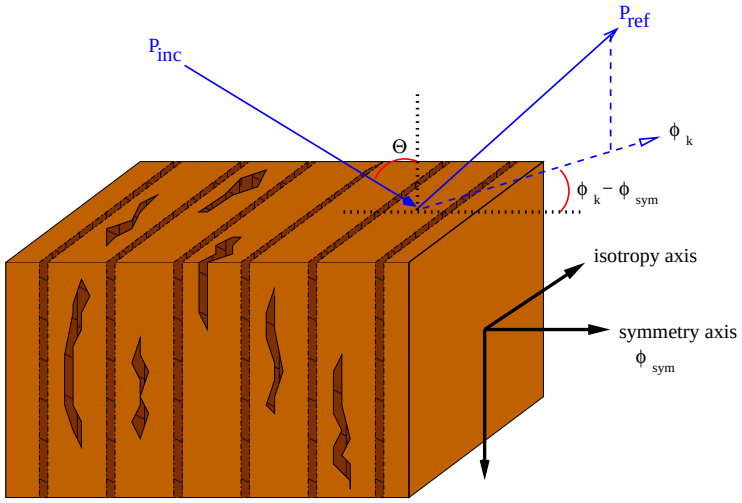

Figure 1: Sketch of HTI model with aligned vertical fractures

These fractures typically have small aspect ratios due to the orientation of local stresses. In the direction of the isotropy axis, these apparently thin fractures have little effect on the elastic properties, and thus reflection amplitudes, compared with the homogeneous case. For ray-paths along the symmetry-axis however, fracture compliance can play a large role in the behavior of reflection amplitudes. This is a manifestation of the rock

and fluid compressibility, density, and fracture geometry. These two directions represent the extremes of the azimuthal AVO behavior, where seismic waves typically propagate more slowly in the fracture normal (symmetry-axis) direction.

An analysis of seismic waves propagating over a 180 degree range of azimuths should therefore sample one complete 'cycle' of this transverse isotropy. The goal of AVOA analysis is to capture the azimuthal variation of reflection amplitudes, which requires data collected at an absolute minimum of three independent azimuths. In practice, wide-azimuth 3D survey methods are required to adequately sample the offset-azimuth space. Reflection amplitudes at a given offset will have an azimuthal dependence that is periodic with respect to the symmetry axis.

Rüger's addition to Shuey's approximation is meant to capture this azimuthal variation in amplitudes. The AVO gradient ('B') term is split into a constant, isotropic term, and an azimuthally varying anisotropic term.

$$B(\phi_k) = B^{iso} + B^{ani}\cos^2(\phi_k - \phi_{sym}) \tag{6}$$

In this equation, ϕ_k represents an arbitrary *known* source to receiver azimuth within the dataset, and ϕ_{sym} represents the *unknown* symmetry-axis orientation. This is a non-linear equation with several terms coupled together. The result of this non-linearity is that there are two possible solutions for B^{ani}. Often, *a-priori* knowledge about the general fracture orientation (or regional stress) can be used to select one of the solutions.

While there will also be an azimuthal variation of the higher angle ('C') term, it will not be developed here. This may be a partial limitation of results shown for larger angles of incidence. Equation 5 can then be written for the azimuthally varying case as:

$$R_{PP} \approx A + [B^{iso} + B^{ani}\cos^2(\phi_k - \phi_{sym})]\sin^2\Theta \tag{7}$$

2.2.1 Linearization of azimuthal AVO approximation

Equation 7 must be linearized before it can be used in a simple least squares inversion. Taking advantage of the two trigonometric identities,

$$\cos^2(\phi_k - \phi_{sym}) = \frac{1}{2}(1 + \cos(2\phi_k - 2\phi_{sym})) \tag{8}$$

$$\cos(2\phi_k - 2\phi_{sym}) = \cos 2\phi_k \cos 2\phi_{sym} + \sin 2\phi_k \sin 2\phi_{sym} \tag{9}$$

this equation can be put into a linear form.

$$R_{PP} \approx A + (B^{iso} + \frac{1}{2}B^{ani})\sin^2\Theta + (\frac{1}{2}B^{ani}\cos 2\phi_{sym})\cos 2\phi_k \sin^2\Theta + (\frac{1}{2}B^{ani}\sin 2\phi_{sym})\sin 2\phi_k \sin^2\Theta \tag{10}$$

Or, it can be written as a linear equation in four unknowns,

$$R_{PP} \approx C_1 + C_2\sin^2\Theta + C_3\cos 2\phi_k \sin^2\Theta + C_4 \sin 2\phi_k \sin^2\Theta \tag{11}$$

which is similar to the approach used by Xu et al. (2001), where

$$\begin{aligned} A &= C_1 \\ B^{ani} &= \pm 2\sqrt{{C_3}^2 + {C_4}^2} \\ B^{iso} &= C_2 - \tfrac{1}{2}B^{ani} \\ \phi_{sym} &= \tfrac{1}{2}\arctan\tfrac{C_4}{C_3} \end{aligned}$$

2.3 Application of Least Squares to AVO

An ordinary least squares inversion can now be used with either equations 5 or 11. These equations are put into a simple linear form,

$$\underline{\underline{E}}\,\underline{\tilde{x}} + \underline{n} = \underline{y} \tag{12}$$

where the solution for the overdetermined problem that minimizes the data residual norm, $||\underline{n}||^2$, is

$$\underline{\tilde{x}} = (\underline{\underline{E}}^T\,\underline{\underline{E}})^{-1}\underline{\underline{E}}^T\,\underline{y} \tag{13}$$

In these linear equations, $\underline{y}$ represents the data, or reflection amplitudes, $\underline{\tilde{x}}$ is the estimate of the AVO model, $\underline{n}$ is the data residual, and the matrix $\underline{\underline{E}}$ is made up of the terms that multiply the AVO parameters. For example, $\underline{\underline{E}}$ matrices for the AVO and AVOA inversions have the following form:

$$\underline{\underline{E}}_{AVO} = \begin{pmatrix} 1 & \sin^2\Theta & (\tan^2\Theta - \sin^2\Theta) \\ 1 & \sin^2\Theta & (\tan^2\Theta - \sin^2\Theta) \\ 1 & \sin^2\Theta & (\tan^2\Theta - \sin^2\Theta) \\ . & . & . \\ . & . & . \\ . & . & . \\ . & . & . \\ 1 & \sin^2\Theta & (\tan^2\Theta - \sin^2\Theta) \end{pmatrix} \quad \underline{\underline{E}}_{AVOA} = \begin{pmatrix} 1 & \sin^2\Theta & \cos 2\phi_k \sin^2\Theta & \sin 2\phi_k \sin^2\Theta \\ 1 & \sin^2\Theta & \cos 2\phi_k \sin^2\Theta & \sin 2\phi_k \sin^2\Theta \\ 1 & \sin^2\Theta & \cos 2\phi_k \sin^2\Theta & \sin 2\phi_k \sin^2\Theta \\ . & . & . & . \\ . & . & . & . \\ . & . & . & . \\ . & . & . & . \\ 1 & \sin^2\Theta & \cos 2\phi_k \sin^2\Theta & \sin 2\phi_k \sin^2\Theta \end{pmatrix}$$

There is one row for every measured reflection amplitude and, typically, the AVO inversion is performed on a single common mid-point (CMP) gather. This results in a linear equation for each trace, where the angle of incidence, Θ, will be different for each offset in the CMP gather at a given depth.

3 Synthetic Analysis

3.1 Ordinary (non-azimuthal) AVO

3.1.1 Description of the model and data

In order to understand the behavior of the least squares analysis, a simple model for the interface between two layers with different elastic parameters is used to create AVO coefficients based on equation 5. This example uses the parameters summarized in table 1. The synthetic AVO coefficients are calculated directly from equations 2 - 4.

From these coefficients, synthetic reflectivity data (R_{PP}) can be calculated over a range of incidence angles commonly found in reflection seismology. The synthetic data can then be contaminated with noise, or partially removed over certain offset ranges, and the ability of the inversion to recover the original coefficients is studied. The modeled behavior for the offset dependant reflectivity is shown in figure 2, where the angles are based on fixed source-to-receiver offsets and a depth to the interface of 800m.

In this figure, the effect of modeling only the A and B terms is clear; there is little deviation below 20°, around 10% at 30°, and then they diverge significantly at larger angles. The three term reflectivity curve will be treated as the 'true' value for the following inversion sensitivity discussions. The effects of changing source-to-receiver geometry is studied using both 2- and 3-term AVO models, as well as their behavior in the presence of noise. For this experiment, random noise with a Gaussian distribution and standard deviation of 0.02 is added to the 'true' reflectivity data. This standard deviation corresponds to about 13% of the mean value of the original model.

	Layer 1	**Layer 2**
V_P	3000 m/s	4000 m/s
V_S	1732 m/s	2309 m/s
ρ	2300 kg/m^3	2600 kg/m^3
σ	0.25	0.25
AVO-A	0.202	
AVO-B	-0.316	
AVO-C	0.143	

Table 1: Elastic parameters for two-layer AVO model

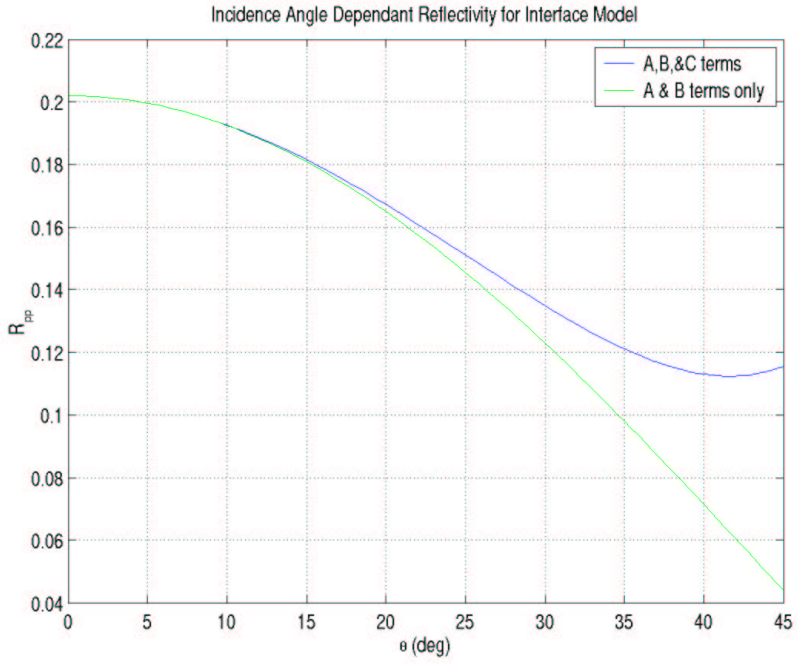

Figure 2: Modeled AVO for a simple two-layer interface using equation 5 and the parameters in table 1

3.1.2 Synthetic AVO tests

The first case, shown in figure 3, uses data sampled from the 'true' reflectivity curve in one degree intervals from 0° to 45°. Using the high angle of incidence data, it is clear that a 2-term AVO model is incapable of recovering the correct values, even for the noise-free case. The fact that the 2-term model is inappropriate can also be seen in the residual, which shows structure. In the presence of noise, the AVO gradient term has an error of 31% for the 2-term model, compared with only 8% for the 3-term model.

Typically, the source-to-receiver offsets and target depths in a seismic survey do not extend all the way to 45°, and this same experiment is repeated using only data from 0° to 30°. These results are shown in figure 4. With noise-free data, the 2-term AVO model is more accurate than before, but is still unable to recover the true solution. When some noise is added to the reflectivity measurements, however, the 2-term and 3-term results are much more similar. By eliminating the far offset data and adding noise, the 3-term solution becomes much less accurate. Repeating this experiment several times with different noise realizations, one finds that the estimate of the 3-term model is unbiased about the correct answer, but has a fairly large standard deviation. The 2-term model estimate does not have the correct mean, but has much sharper resolution.

Finally, for a more representative approximation of real acquisition geometries, information about the near offsets is also removed, so that the data lies between 10° and 30°. An example of the least squares solution for a single noise realization is shown in figure 5. Repeating this experiment several times, one again finds that the 2- and 3-term AVO solution estimates involve sacrifices between resolution and the accuracy.

3.1.3 Discussion of results

Another useful way to compare the effects of these geometries is through the use of a resolution matrix. Resolution matricies for three of the examples are shown in figure 6. It is clear that as information is removed from the data, the model parameters become more dependent on an broader set of measurements. In the 3-term case, it seems that there is a more dramatic linear dependence of measurements, which is likely the reason why a little noise in the data can produce more spurious results.

These three simulations are useful in understanding the relationship between the AVO model being used, survey geometry, and the presence of noise. Without performing a more rigorous statistical analysis of the results, one might conclude that the 2-term AVO model is robust for use with typical seismic datasets. This reliability does not come for free however, as there is some sacrifice in resolution.

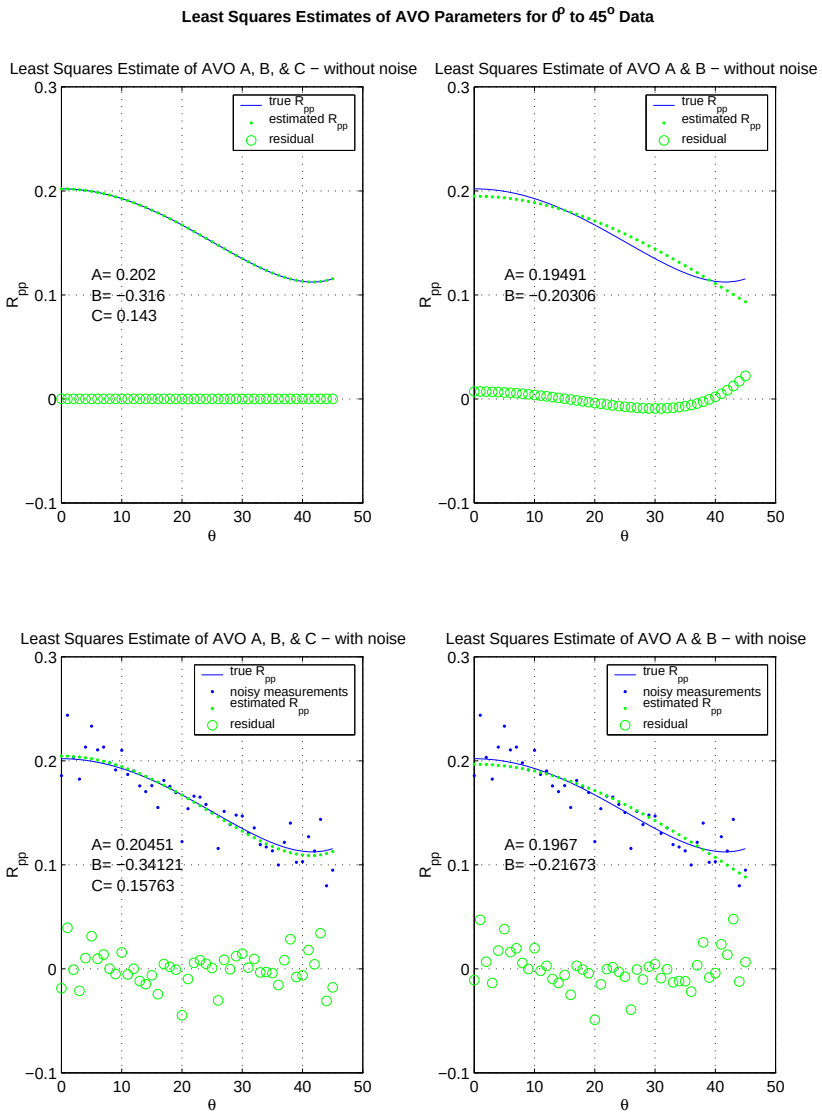

Figure 3: AVO inversion results for the two-layer model using data from 0° to 45°

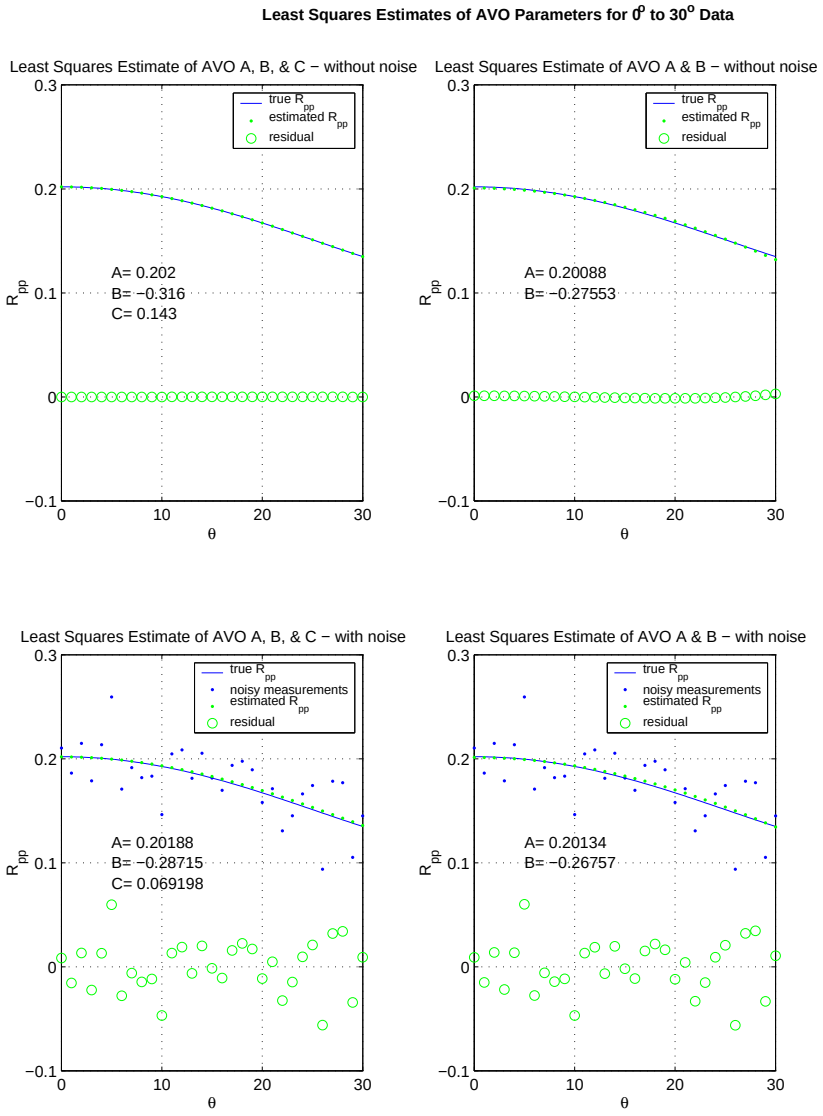

Figure 4: AVO inversion results for the two-layer model using data from 0° to 30°

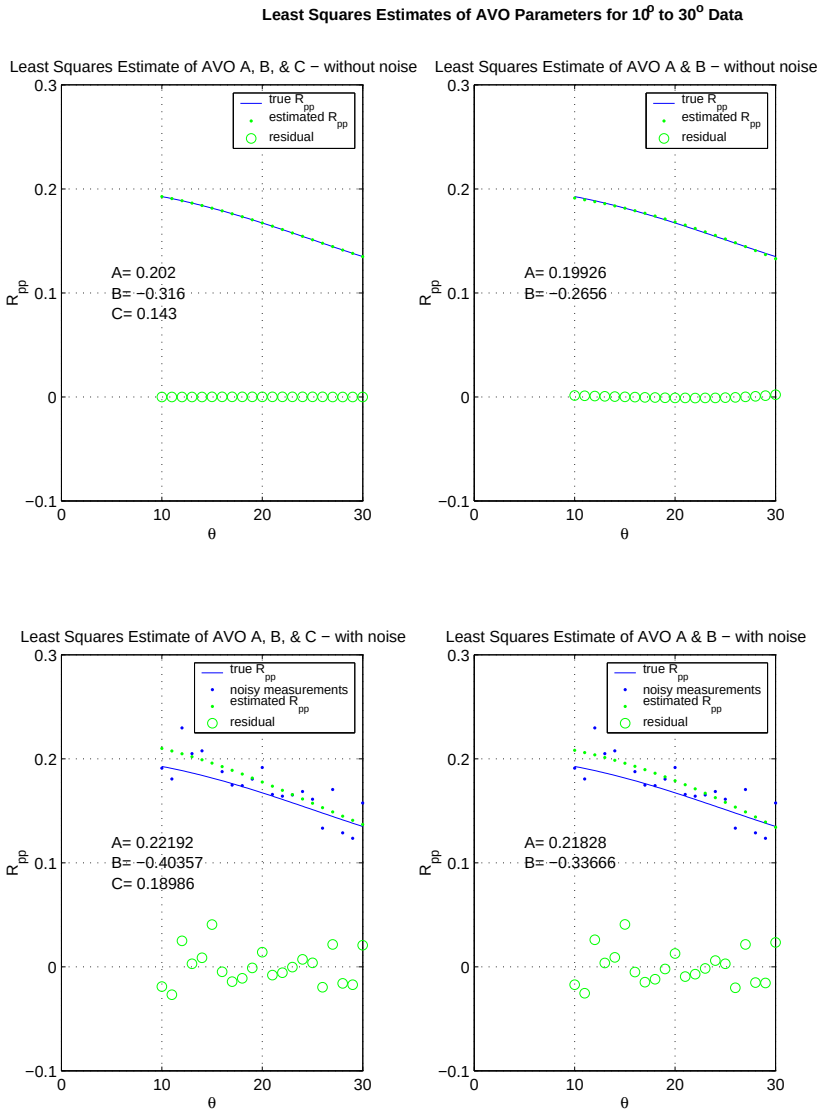

Figure 5: AVO inversion results for the two-layer model using data from 10° to 30°

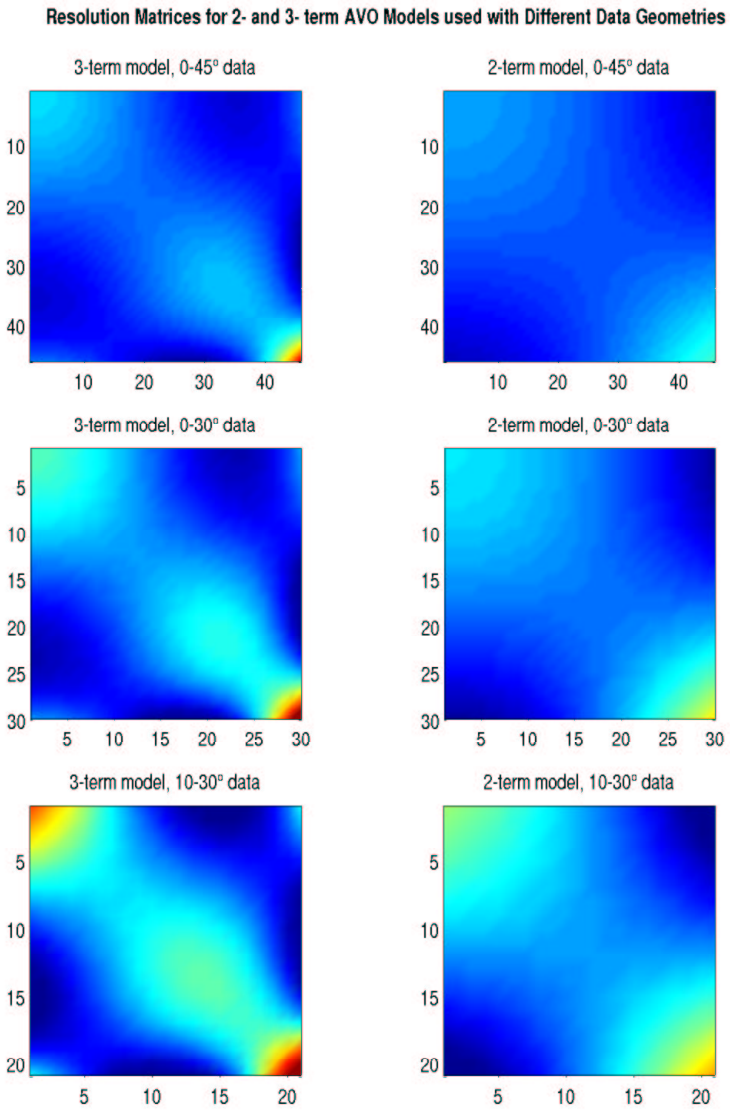

Figure 6: Resolution matrices for the least squares method using 2- and 3- term AVO models and three different cases of source-receiver geometry. N.B. Color scales are all the same

3.2 Azimuthal AVO

3.2.1 Description of the model and data

A similar synthetic analysis can be preformed using azimuthal AVO, where equation 7 is used to create the 'true' R_{PP} reflectivity model. Synthetic data is created from this model by decimating the offset-azimuth space to represent a realistic survey geometry, and by adding random noise. The data is then used with equation 11 in a least squares setting to find the azimuthal model parameters $A, B^{iso}, B^{ani}, and\, \phi_{sym}$. Construction of the $\underline{\underline{E}}$ matrix is similar to the previous section, though there are now four columns, with dependence on incidence angle *and* azimuth.

Two synthetic models are investigated using evenly distributed datasets with slightly different geometries (an example of which is shown in figure 7), and a third model will simulate the true 3D survey geometry associated with the OBC data discussed at the end of the report. This analysis will be a good calibration tool for the results obtained when working with the actual field data. In each case, Gaussian noise with standard deviation of 0.05 is added to the 'true' R_{PP} measurements. This standard deviation corresponds to about 33% of the mean value of the noise-free data.

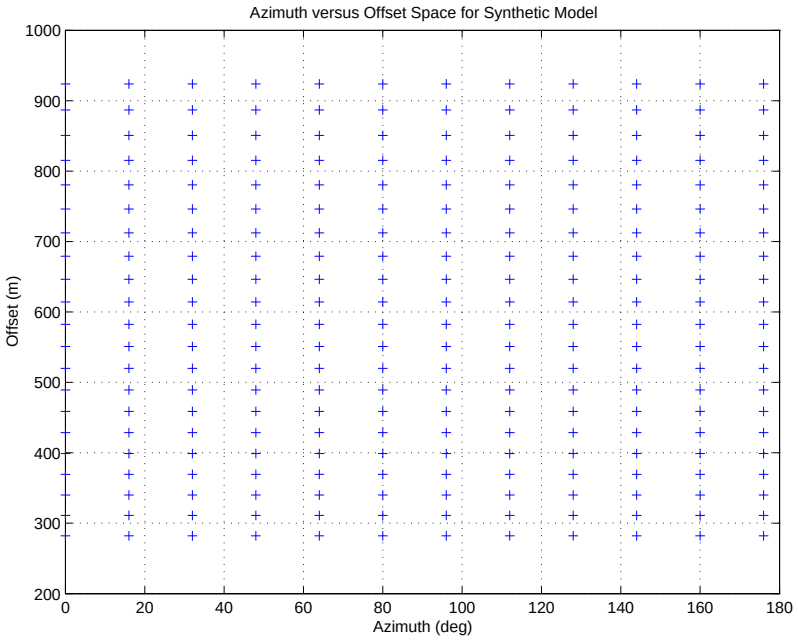

Figure 7: Azimuth-offset geometry used for synthetic AVOA analysis

For consistency with the non-azimuthal AVO analysis, the same elastic model parameters are used, with some slight modifications for the azimuthal case. The AVO-A term is unchanged, as it does not vary with azimuth. The AVO-B term is split into two parts, where 80% of the value used in the previous section is assigned to B^{iso}, and 20% to B^{ani}. An arbitrary fracture symmetry-axis orientation of 35° is used. The 'true' model parameters for the azimuthal analysis are summarized in table 2

A	0.202
B^{iso}	-0.2528
B^{ani}	-0.0632
ϕ_{sym}	35°

Table 2: True AVOA model parameters for two-layer azimuthal AVO model

The 'true' reflectivity behavior, based on equation 7 is shown in figure 8 for a few selected azimuths. In this figure, the azimuthal behavior of the AVO gradient term is apparent. At azimuths closest to the fracture symmetry axis (35°), the greatest curvature is seen (blue and green curves) due to the contribution of the B^{ani} term. The least squares inversion aims to capture this behavior in order to uniquely and accurately determine the four model parameters.

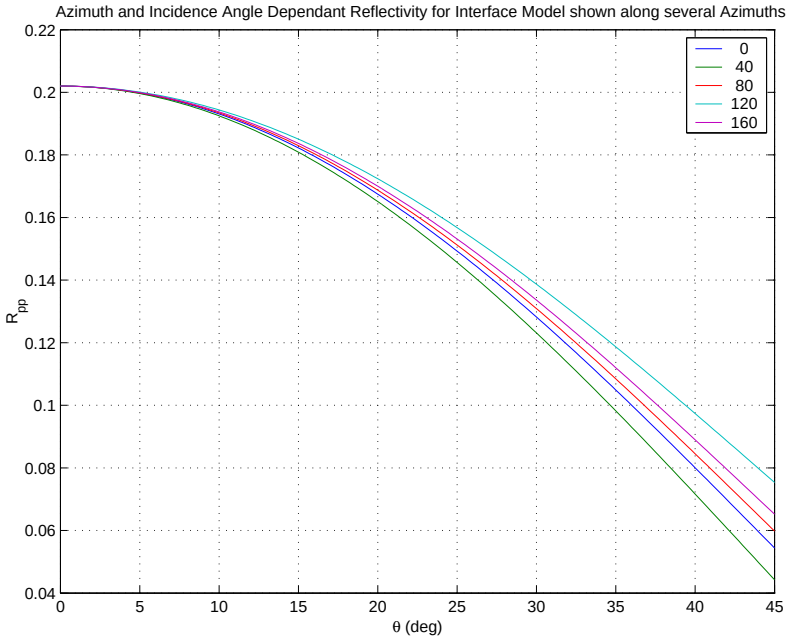

Figure 8: Synthetic AVOA model curves for several azimuths based on the parameters in table 2

3.2.2 Synthetic AVOA tests

The first test of the four-term least squares inversion method is really a validation, as the input data comes from an even distribution of offsets and azimuths. The synthetic reflection amplitudes are sampled at a one degree spacing between 0° and 45° in incidence angle, and at every four degrees between 0° and 180° in azimuth. This dataset is inverted for the four AVOA model parameters using equation 11 and the subsequent relationships between coupled terms. The inversion is repeated with 2000 realizations of the random noise, and the average results are summarized in table 3. Note that the noise-free example has perfectly resolved the model, which should be expected since it is using a linearized form of the same model that created the data. The inversion of the noisy data has been distorted somewhat, but the AVOA parameters have been resolved within reason.

Next, only the data with angles of incidence between 10° and 30°, and azimuths separated by 16° (figure 7), are used in the same inversion process to simulate a more realistic survey geometry. Again, the average results are summarized in table 3. There is clearly a significant loss of accuracy in the inverted model when the offset-azimuth space is this sparse.

Finally, the same method is used with an offset-azimuth distribution that comes from data collected during an OBC survey. This distribution is shown in figure 10 and, though it is dense, it is not as uniformly sampled as the synthetic cases. As can be seen in table 3, this survey geometry has performed somewhere in-between the previous two synthetic models.

parameter	true value	without noise	all offsets/azimuths	sparse offsets/azimuths	OBC geometry
A	0.202	0.202	0.2019	0.2022	0.205
B^{iso}	-0.2528	-0.2528	-0.2517	-0.2378	-0.2609
B^{ani}	-0.0632	-0.0632	-0.0645	-0.0962	-0.0621
ϕ_{sym}	35°	35°	34.8°	57.1°	40.1°

Table 3: Average results of azimuthal AVO inversions using noisy synthetic data for different geometries and 2000 noise realizations

3.2.3 Discussion of results

The four-term azimuthal AVO inversion method seems to have the fundamental ability to resolve azimuthally varying features in seismic data. The combination of survey geometry and noise content are two of the major controlling factors in the success of this approach, and can clearly lead to suprious results. A more rigorous statistical analysis of various geometries and levels of noise would be a very useful tool with regards to the adequacy of AVOA analysis for a specific dataset, data preparation, and interpretation of inversion solutions. For example, an optimal scheme of offset-azimuth selection and trace stacking to suppress noise can be chosen for a specific dataset based on these statistical conclusions. It is also possible that a weighted least squares inversion could be developed based on these results that would be more appropriate for use with AVOA.

4 Field data analysis

In an attempt test the lessons learned throughout this study, some field seismic data collected during an OBC survey will be analyzed. This survey is known to cover regions of oriented vertically aligned fractures, which will help to test the argument for using AVOA in the detection of HTI features. A comparison of the AVOA inversion results with known fracture parameters will provide a useful calibration for this method.

4.1 Data overview

As already discussed, one of the fundamental requirements for use in AVOA analysis is an acquisition geometry that covers a wide range of offsets and azimuths. A more detailed discussion of the geometry adequacy is addressed in Dong and Davidson (2003). The reason for choosing this OBC survey is that it contains data over a full range of azimuths, with offsets ranging from a few hundred meters to over 4000 meters. The offset-azimuth distribution for an 8-by-8 block of CMPs is shown in figure 9. This block of CMP data will be used in the following AVOA analysis.

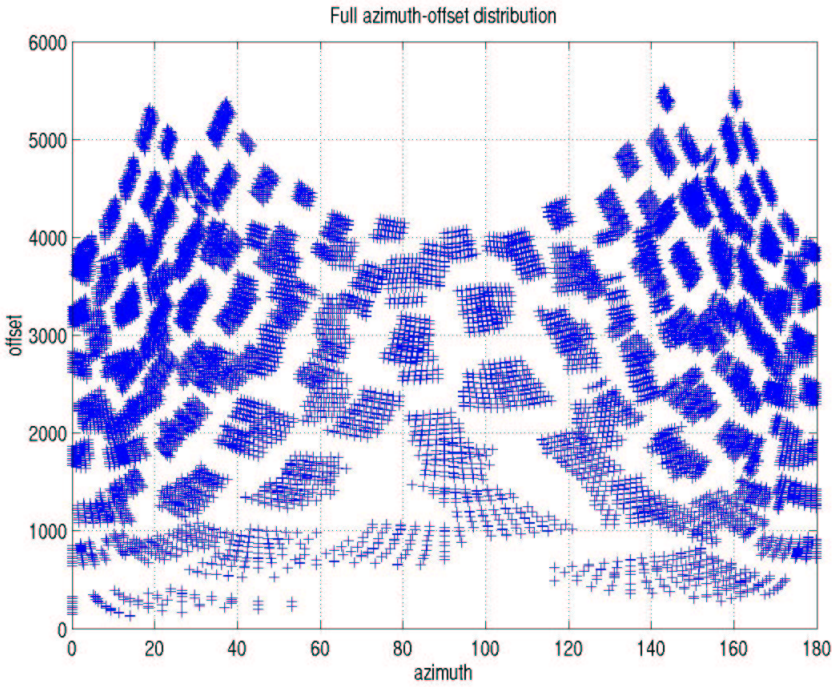

Figure 9: Offset-azimuth distribution for all traces that fall within an 8 x 8 super-CMP bin

One of the major problems commonly found with analyzing field data is noise. Because AVO analysis is performed on pre-stack data, it is often difficult to obtain a good signal-to-noise ratio; therefore, the pre-processing steps meant to enhance the signal must also be careful not to distort the natural AVO behavior. For this reason, it is common to analyze more than one CMP at a time, and to stack traces with common offset-azimuth values. While this will have the effect of blurring true amplitudes across offset-azimuth space, it is a necessary step in overcoming the noise problem. Before performing the azimuthal AVO analysis on this super-CMP gather, a few steps are taken to enhance the signal, while regularizing the data space used in the analysis.

4.2 AVOA analysis of field data

There is an obvious clustering of the traces in the block of CMPs shown in figure 9, which is more dense near zero and 180 degrees. The traces are first smoothly discretized in this offset-azimuth space so that the solution is not biased towards azimuths with more data points, and to reduce the overall volume of data. The criteria for discretizing the traces is such that only one trace is accepted in any offset-azimuth bin with dimensions of $1m\,by\,30°$. The resulting CMP dataset is shown in figure 10. The CMP gather corresponding to this set of traces is shown in figure 11. The reason for the odd appearance at the bottom of the record is due to the Normal Moveout function applied to the data, and is not included in the AVO analysis.

The traces in the super-CMP are now sorted into common-azimuth gathers, which are shown in figure 12. The azimuth bins are each 30 degrees wide, and are annotated with the orientation of the center of each bin. At this point, common offset stacking is applied within the azimuth gathers to enhance the signal. This involves stacking all of the traces within 100m offset groups for each azimuth gather. Besides helping to improve the signal-to-noise ratio, common offset stacking has the benefit of regularizing the offsets that are input into the inversion.

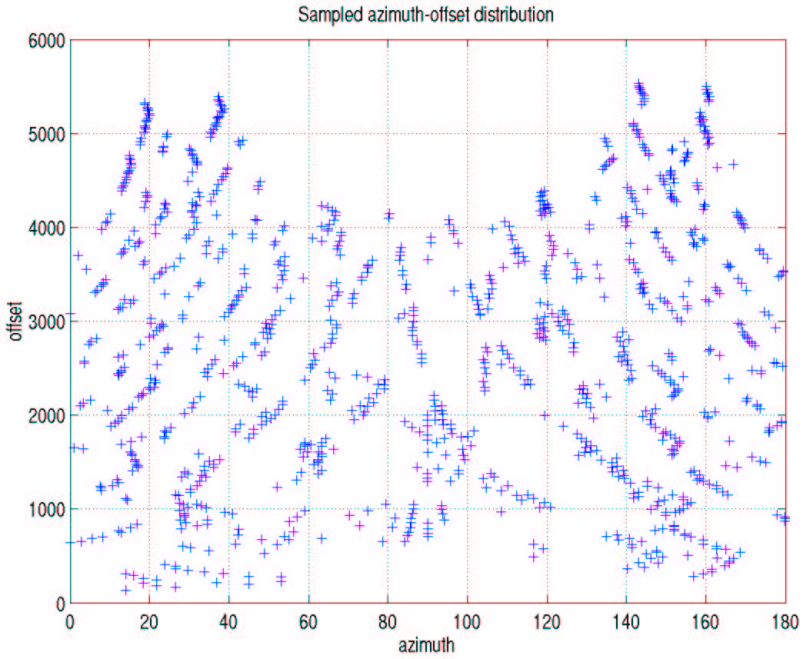

Figure 10: Regularized offset-azimuth distribution for traces in $1mx30°$ bins

These azimuth gathers now contain all of the information used as input for the AVOA analysis. Using local velocity information, the time axis can be converted into approximate depths. Along with the known offsets for each trace, approximate angles of incidence can be calculated, though ray-tracing would be required for a more accurate representation. With known angles of incidence and source-to-receiver azimuths, the $\underline{\underline{E}}$ matrix can be computed with the same procedure as with the synthetic example. For a single time horizon in the gather, amplitudes are collected from all of the traces and are used as the observations in equation 11. The associated resolution matrix for this setup is shown in figure 13, and it reveals that that there is a strong interdependence of measurements over several different azimuths.

The least squares inversion will produce a set of values for the four AVOA model parameters at any given time step. Sliding down the trace in incremental steps of 20ms, this analysis is repeated at each time, and the results are collected for the gather between 1 and 3 seconds. A log-type display of the four parameters versus time is shown in figure 14.

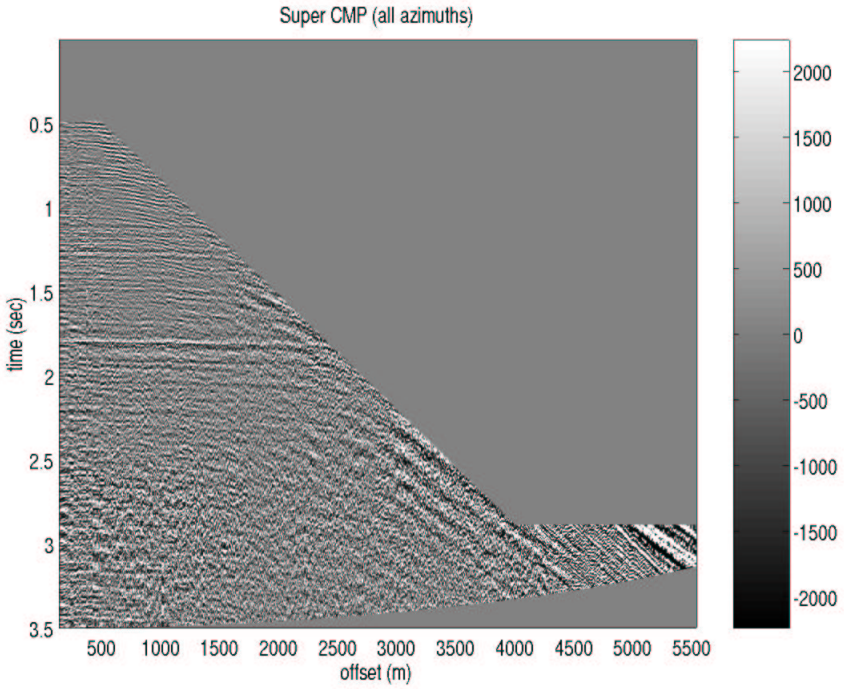

Figure 11: CMP display of the traces to be used in AVOA analysis

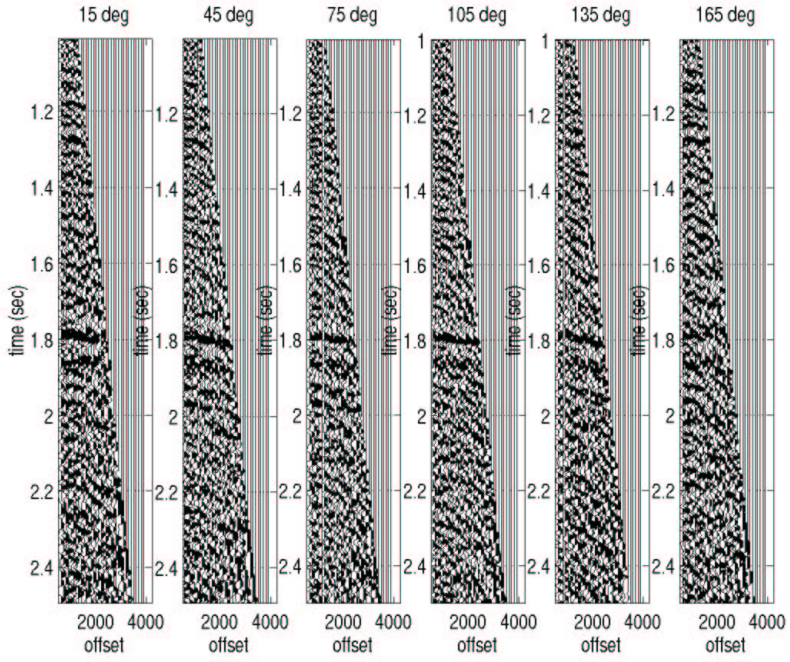

Figure 12: CMP traces sorted into 30 degree azimuth gathers and stacked on common offsets

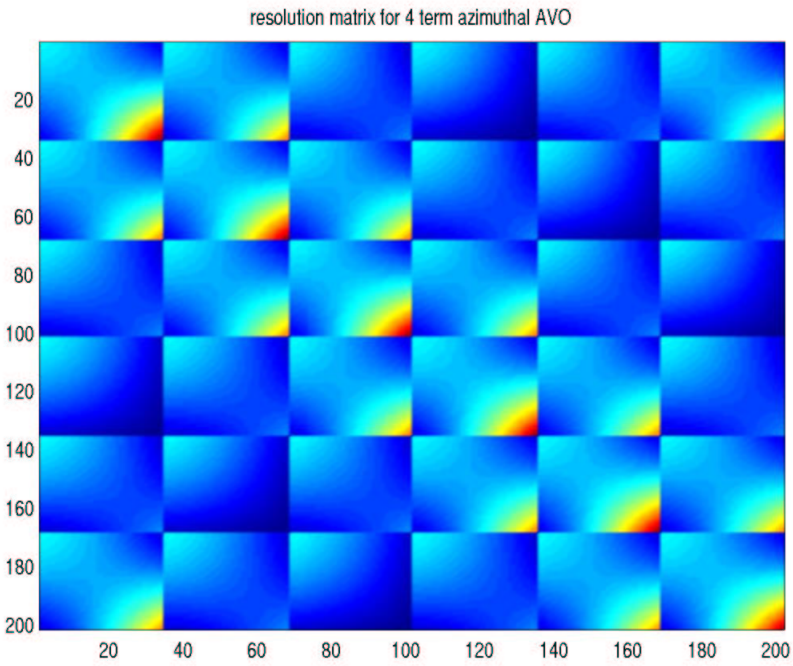

Figure 13: Resolution matrix for the AVOA inversion used on data collected in azimuth gathers

4.3 Discussion of the field data inversion

While this solution represents only a tiny subset of the OBC data, and uses a simple criteria for data selection and stacking, there are some promising results. Probably the most outstanding feature is the alignment of the symmetry-axis orientation near zero degrees between 1.7 and 2.2 seconds. This solution corresponds fairly well with the time and orientation of a known fractured zone. The fact that the solution for ϕ_{sym} is much more focused in this window than it is for earlier or later times suggests that the inversion is capable of resolving features within the data. It is difficult to comment on the behavior of the other parameters however, as there are no other similarly striking trends. This may be related to several factors; including the method of data selection/stacking, the non-uniqueness of the B^{ani} solution (which was always forced to be positive for this example), and estimation of the incidence angle based on average velocities.

Further effort towards improving the inversion method is certainly justified, and should help to reveal more information about the other model parameters. The B^{ani} term should also be well correlated with fracture zones, as it captures the difference in AVO behavior between the fracture-normal and fracture-parallel orientations. Isotropic zones should therefore have a small B^{ani}, while fractured regions should have proportionally larger values. B^{iso} will be key in describing the actual differences in material properties at an interface, but is more subtle, and has the draw-back of being coupled to the non-unique solution of the anisotropic term. Finally, one would like to see a decrease in the RMS of the data residual in areas where strong fracturing produces a good fit to the inversion. The reason for the general increase in this RMS curve after 2.2 seconds is likely due to the increased noise in the data at depth. This does not necessarily imply a poor solution, but the probability of a good fit is certainly decreased.

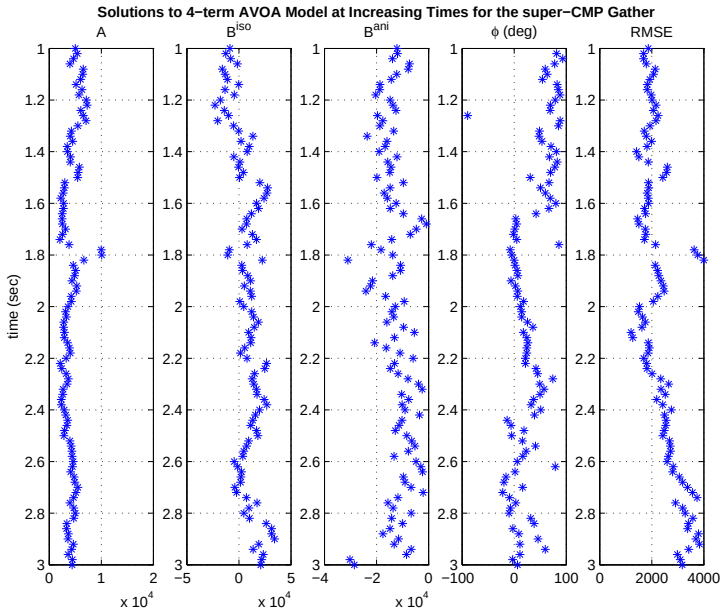

Figure 14: Azimuthal AVO parameter estimates at multiple depths for the OBC super-CMP dataset

5 Conclusions

5.1 AVOA as a tool for fracture characterization

This study has attempted to show the limiting factors that play a role in the ability to resolve factrue information using azimuthal AVO with typical datasets. The synthetic and field data analysis presented here supports the use of AVOA for fracture characterization, though this tool should be considered on two levels. The first of these levels is the ability to detect and spatially map oriented fractures, and to describe basic features such as strike angle and degree of anisotropy. A second, more involved, level is to use the AVOA information to conclude something about the physical properties of the fractures and saturating fluid.

It is important to take into account the limitations and assumptions made with this method however, as the results can be biased significantly due to geometric and noise-related factors. This approach was directed entirely towards describing HTI-like features, which may not be appropriate in all cases. Azimuthal analysis of field data without sufficient constraining information can result in a non-unique solution, and should be interpreted as such.

5.2 Future improvements

There are a few areas of improvement to be addressed that may significantly improve this azimuthal AVO inversion method, providing a much stronger fracture characterization tool. A few of these include: better estimates of the incidence angle with depth, *a-priori* constraints on the values of ϕ_{sym} and sign of B^{ani}, statistical analysis of the inversion behavior with various geometries and levels of noise (possibly leading to a weighted inversion), optimization of the data discretization/stacking method, and extension of the model beyond HTI. Analysis of numerical model output with controlled fracture properties should also prove useful as a calibration tool for this technique.

6 Acknowledgements

This work was supported by the Earth Resources Laboratory Founding Members, the Department of Energy grant number DE-FC26-02NT15346, and by ENI S.p.A. AGIP.

References

Aki, K. and Richards, P. G. (1980). *Quantitative Seismology: Theory and methods*. W.H. Freeman and Co.

Castagna, J. P. (1993). Avo analysis - tutorial and review. In *Offset-Dependent Reflectivity: Theory and Practice of AVO Analysis*, pages 3–36, Tulsa. Society of Exploration Geophysicists.

Dong, W. and Davidson, M. E. (2003). Quantifying 3d acquisition adequacy for azimuthal avo analysis. *The Leading Edge*, pages 476–480.

Mallick, S., Craft, K. L., Meister, L. J., and Chambers, R. E. (1998). Determiniation of the principal directions of azimuthal anisotropy from p-wave seismic data. *Geophysics*, 63(2):692–706.

Pérez, M. A., Gibson, R. L., and Toksöz, M. N. (1999). Detection of fracture orientation using azimuthal variation of p-wave avo responses. *Geophysics*, 64(4):1253–1265.

Rüger, A. (1997). P-wave reflection coefficients for transversely isotropic models with vertical and horizontal axis of symmetry. *Geophysics*, 62(3):713–722.

Rüger, A. (1998). Variation of p-wave reflectivity with offset and azimuth in anisotropic media. *Geophysics*, 63(3):936–947.

Shuey, R. T. (1985). A simplification of the zoeppritz equations. *Geophysics*, 50(4):609–614.

Xu, Y., Pickford, S., and Li, Y. (2001). Uncertainties in azimuthal avo analysis. In *The Labours of Hercules II, AVO and AVO Reliability II*, pages 24–27. Canadian Society of Exploration Geophysicists.